Colloid Polym Sci (2008) 286:59–65
DOI 10.1007/s00396-007-1686-9

ORIGINAL CONTRIBUTION

Wetting and non-wetting fluids in surface-functionalised activated carbons

Krisztina László · Orsolya Czakkel · Erik Geissler

Received: 9 February 2007 / Accepted: 25 April 2007 / Published online: 22 May 2007

Abstract Pore filling by non-polar and polar molecules is investigated by small-angle X-ray scattering in activated carbons that had been surface-functionalised to different degrees by oxidation. A pseudo-binary model for the scattering response is used to trace the filling characteristics of water and n-hexane in the pore structure. While the pores are uniformly filled by n-hexane, pore filling by water is only partial. In the latter case, a significant contribution from liquid–vapour interfaces appears and the system becomes fully ternary. This feature is direct evidence of the development of water droplets, which form even in the most oxidised carbon. The appreciable differences between the carbons illustrate the influence on the small-angle X-ray scattering response of surface chemistry and of the polarity of the adsorbed molecules.

Keywords Activated carbon · Surface treatment · Small-angle X-ray scattering · Interfacial properties

Introduction

Carbon has been used for millenia as a multi-purpose adsorbent by virtue of its high affinity towards a wide diversity of chemical species. Recognition of the role of surface area and pore hierarchy in the performance of porous carbon has stimulated the commercialisation of carbon adsorbents with tailor-made porosity [1–3]. Their design at the nanoscale level has revealed the importance of an additional basic parameter, namely, the surface chemistry, by which the adsorption capacity of the complex pore network can be further enhanced. In adsorption processes, the affinity between the carbon surface and the fluid phase plays a major role, as their generally non-specific interaction significantly affects the distribution of the adsorbed molecules within the pores. Introduction of heteroatoms into the turbostratic layers renders the carbon surface more attractive to polar molecules. The most frequent heteroatom in the carbon matrix is oxygen, which is generally bonded along the edges of the graphene layers.

In this paper we investigate the influence of the chemical character of both the adsorbent and the adsorbate on the wetting by systematically varying the surface chemistry of the sample and the nature of the interacting fluid. The interaction of carbon samples of increasing oxygen content, i.e., increasing polarity, is studied with two different probe molecules. The non-polar molecule n-hexane is attracted to carbon through a strong dispersion interaction, which favours significant adsorption already at low relative pressures p/p_0. Water molecules, which interact only weakly with graphitic carbon surfaces, adsorb on the carbon surface by a different mechanism [4, 5]. Hydrogen bonding, however, gives rise to strong fluid–fluid interaction among the water molecules. Surface oxygen functionalities offer the possibility of hydrogen bonding with the surface and, by this mechanism, facilitate the adsorption of water molecules. The surface functional groups thus act as nucleation centres that, upon further accretion, ripen into clusters at p/p_0 as low as 0.1 [6]. While pore filling occurs already at low p/p_0 in the case of non-polar adsorbates, for water it does not begin until about

K. László (✉) · O. Czakkel
Department of Physical Chemistry and Materials Science,
Budapest University of Technology and Economics,
H-1521 Budapest, Hungary
e-mail: klaszlo@mail.bme.hu

E. Geissler
Laboratoire de Spectrométrie Physique CNRS UMR 5588,
Université J. Fourier de Grenoble,
BP 87, 38402 St Martin d'Hères cedex, France

p/p_0=0.5. For higher relative pressures, however, the Dubinin–Astakhov equation yields excellent fits to the isotherm [7]. At very low surface coverage, water adsorption is governed both by the surface chemistry and by the porosity of the carbons. Water uptake in the carbon may be enhanced at low p/p_0 by introducing oxygen functionalities because surface sites can, through a cooperative bonding mechanism, have the same effect as pre-adsorbed water [8].

Under real operating conditions, the relative humidity (RH) of the environment often places water in competition with other target molecules for adsorption sites. Water, which is of particular relevance in activated carbon–vapour phase interactions, is therefore used as the polar probe.

Small-angle X-ray scattering (SAXS) or neutron scattering furnishes structural information about the adsorbent–adsorbate system in the nanometre scale range. Because molecules adsorbed inside the pores modify the electronic contrast of their immediate surroundings, the small-angle scattering signal of the local carbon matrix is sensitive to the adsorbed layer [9–13]. Contrast variation scattering techniques make use of this phenomenon.

The present article describes SAXS measurements on activated carbon samples of well-characterised surface morphology and chemistry. As the SAXS response is related to spatial distances through the transfer wave vector q, the pore-filling by the adsorbed molecules can be conveniently translated into the pore size w as $2\pi/q$. Such observations yield model-independent information about pore filling by any adsorbed molecule.

Experimental

Preparation and characterisation of the carbon samples

To avoid inorganic impurities from the raw materials, the samples described in this paper were prepared from a polymer precursor and were chemically modified to varying degrees by oxidation with nitric acid. Granular activated carbon was prepared from poly(ethylene terephthalate) pellets (APET) [14]. Steam-activated carbon, obtained at 900 °C, was treated for 3 h with concentrated nitric acid at room temperature (APETA) and at the boiling point of the carbon–acid suspension (APETB) to achieve different degrees of surface functionalisation. Before use, these acidic samples were washed with distilled water and extracted in a Soxhlet apparatus until neutral pH was attained. The surface chemistry and morphology of these carbons have been characterised elsewhere [15, 16].

Nitrogen adsorption/desorption isotherms, measured at 77 K with a Quantachrome Autosorb-1 instrument, were also discussed previously [16]. The surface areas obtained from the Brunauer–Emmett–Teller and the Dubinin–Radushkevich models for APETA lie in the range 1,100–1,300 m^2/g. For APETB, however, the hot nitric acid treatment reduced the surface area by 75% to less than 350 m^2/g, but the pore size distribution in the micropore range nevertheless remained practically unaffected. Average pore widths, derived from the ratio of the total pore volume to the surface area assuming slit-shaped geometry, were 8.6 and 9.2 Å for APETA and APETB, respectively. The true densities d_{He} of the same samples, determined by helium pycnometry with the AUTOSORB-1 instrument, were 1.82 and 1.50 g/cm^3.

Water vapour adsorption isotherms were measured on a Hydrosorb apparatus (Quantachrome) at 20 °C. Hexane uptake at p/p_0=0.4 was determined at 20 °C by gravimetry, using an n-hexane/n-dodecane mixture to set the desired relative pressure.

X-ray photoemission spectroscopy analysis of the surface chemistry in the powdered samples [17, 18] showed a strong increase in the O/C atomic ratio, from 10 to 27%, for APETA and APETB, respectively. The close similarity found between the populations of the different functional groups in the granular and the powdered samples was proof that the chemical treatment acted uniformly throughout the internal surfaces.

Small-angle X-ray scattering

X-ray scattering measurements on the BM2 beam line at the European Synchrotron Radiation Facility, Grenoble, France, were made at two different wavelengths, λ_0= 1.57 Å and 0.69 Å, with sample-detector distances 158, 27, and 6 cm. An indirect illumination CCD detector (Princeton Instruments) with 50-μm effective pixel size was used. Intensity curves $I(q)$, obtained by azimuthal averaging, were corrected for grid distortion, dark current, sample transmission and variations of the incident beam intensity, as well as for background scattering.

The powdered samples, ground in a ball mill to about 0.3 mm particle size, were inserted into 1.5-mm-diameter Lindemann glass capillaries and heated to 110 °C for 24 h to remove trapped or adsorbed water. The capillaries were equilibrated in air containing water vapour at various degrees of RH and then sealed. Other samples were exposed either to liquid hexane or to hexane vapour at 40% partial vapour pressure at 20 °C for 2 weeks before sealing. Intensities were normalised with respect to a standard (lupolen), assuming an effective sample thickness of 1 mm to account for the filling factor of the powder in the capillary tubes. The SAXS measurements were performed at the same temperature as the sample preparation (20 °C).

The intensity of X-rays of wavelength λ scattered through an angle θ by a carbon sample in dry air is

governed by the structure factor of the carbon, $S_1(q)$, and the difference between the electron density of the carbon, ρ_C, and that of air. Thus,

$$I_1(q) = r_0^2 \rho_C^2 S_1(q) \quad (1)$$

In Eq. 1, $r_0 = e^2\mu_0/4\pi m$ is the classical radius of the electron, e and m being the electron charge and mass, respectively, and μ_0 being the magnetic permittivity of space. The magnitude of the transfer wave vector for X-rays is $q = (4\pi/\lambda)\sin(\theta/2)$. The electron density of the carbon is

$$\rho_C = Zd_{He}N_A/M \quad (2)$$

where Z is the atomic number, M the atomic mass, d_{He} the helium density of the sample, and N_A Avogadro's number. The presence of light heteroatoms such as oxygen does not alter the above definition of the electron density of the carbon, as their ratio Z/M is identical. Only the helium density d_{He} is affected by their presence. Although the same argument does not apply to hydrogen owing to its larger value of Z/M, its contribution is negligible because it contains few electrons. The value of ρ_C is therefore determined essentially by the mass density of the carbon. In Eq. 1, the electron density of the surrounding air does not appear as it is much smaller than ρ_C.

If the same sample is impregnated with a fluid that does not completely fill all the unoccupied space in the carbon, then in general, the scattered intensity becomes that of a ternary system, namely,

$$I_{tern}(q) = r_0^2\left\{(\rho_C - \rho_l)^2 S_{cl}(q) + \rho_C^2 S_{cv}(q) + 2\rho_C(\rho_C - \rho_l)S_{lv}(q)\right\} \quad (3)$$

where $S_{cl}(q)$ is the partial structure factor describing the relative positions of carbon and liquid, $S_{cv}(q)$ is that between carbon and vapour phase, and $S_{lv}(q)$ is that between liquid and vapour phase. For the present purposes, it may be assumed that the electronic density of the vapour phase is negligible with respect to that of the liquid and, therefore, is equivalent to a vacuum. Owing to the dispersed nature of micropores in carbons, however, in many cases, the effective liquid–vapour interface is very small and the regions in the carbon in which the fluid is condensed are physically separated from those in which only the vapour phase is present. In such a situation, the last term in Eq. 3 is negligible and the first two terms can be represented by a pseudo-binary expression of the form

$$I_2(q) = r_0^2(\rho_C - \rho_S)^2 S_2(q). \quad (4)$$

in which it is understood that the $(\rho_C - \rho_S)^2 S_2(q)$ is an average over the regions in the sample where the fluid is condensed and where it is not. Because these two regions generally have different characteristic sizes and therefore contribute to different parts of q space, it becomes reasonable to attribute a q dependence to ρ_S, i.e., $\rho_S(q) = p(q)\rho_l$, where ρ_l is the density of the condensed fluid and $p(q)$ is the relative electronic (or mass) density of the fluid with respect to its bulk value. Provided the fluid does not alter the structure of the carbon, $S_1(q)$ and $S_2(q)$ both describe the same total structure factor of the carbon, and hence, $S_1(q) = S_2(q)$. If the pores are uniformly filled, then the two signals $I_1(q)$ and $I_2(q)$ are everywhere proportional to each other, i.e., ρ_S and $p(q)$ are independent of q. If, however, the fluid is not uniformly distributed, e.g., molecules condense only in the finest pores while remaining in the vapour state elsewhere, then the deviations from uniform filling may be expressed in terms of the intensity ratio

$$u(q) = I_2(q)/I_1(q) = [\rho_C - p(q)\rho_l]^2 \Big/ \rho_C^2 \quad (5)$$

and hence,

$$p(q) = \rho_C\left[1 - u(q)^{1/2}\right] \Big/ \rho_1 \quad (6)$$

In principle, $0 \le p(q) < 1$ when the pores are incompletely filled, but $p(q)$ can exceed unity due to strong interaction between the surface and the adsorbed layer. Experimentally, the samples exposed to air or vapour should be strictly equivalent, i.e., the effective thickness of the two samples must be the same. In this model-independent approach, the two basic requirements are that the carbon structure should not be altered by the adsorbed molecules and that the test sample and the dry reference should be equivalent. Apparently, negative values of $p(q)$ may occur due to structural change in the presence of the

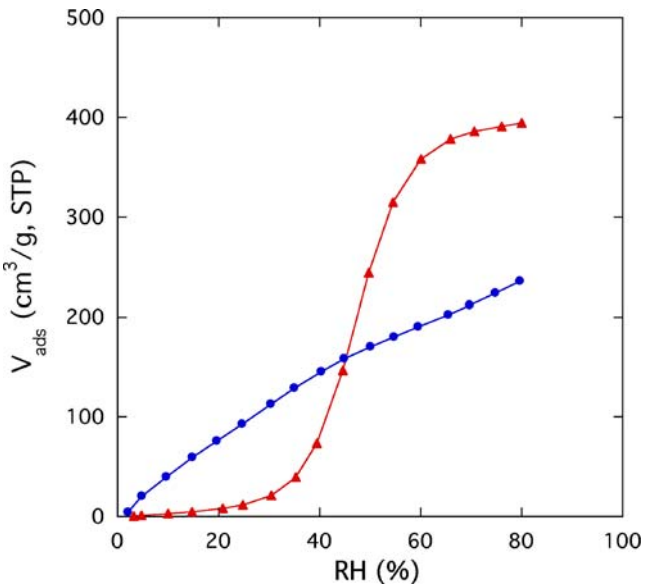

Fig. 1 Water vapour adsorption isotherms for APETA (*triangles*) and APETB (*circles*), measured at 20 °C

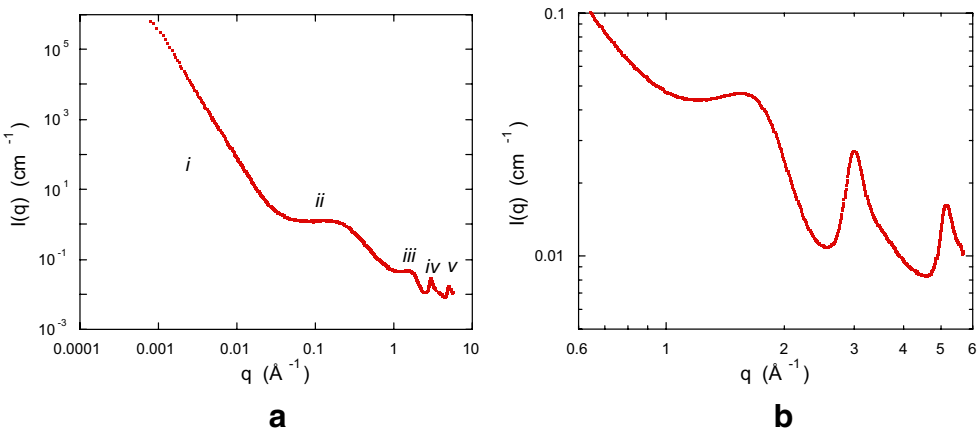

Fig. 2 **a** SAXS spectrum of dry sample APETA indicating regions *i*–*v* described in the text; **b** expanded view of high-*q* response of the same sample, covering the zone in which Bragg reflections are found in graphite. Absence of Bragg reflections shows that the carbon is fully amorphous

adsorbent [$S_1(q) \neq S_2(q)$] or to surface contamination of the reference sample. Strongly negative values of $p(q)$, however, have to do with the source of extra scattering that is neglected in the above pseudo-binary model of independent scattering regions. Thus, in a fully ternary system, extra scattering is generated when extended regions of contact exist between the condensed solvent and its vapour, e.g., in the form of separate clusters or droplets.

Results and discussion

Non-polar molecules like hexane yield an isotherm on carbons that is initially convex. At 20 °C with p/p_0=0.4, hexane uptake is 0.29 and 0.08 g/g in APETA and APETB, respectively. The shape of the water isotherm, however, is sensitive to the extent of oxidation of the carbon. The water vapour isotherms in Fig. 1 reveal that the type V isotherm of APETA transforms to type IV due to the acidic treatment.

Figure 2 illustrates the SAXS spectrum from the dry APETA sample, measured over the extended range of q available on beam line BM2. The equivalent spectrum of the APETB is not shown, as it is almost indistinguishable at this scale. For clarity, the figure is divided into five regions: In region i, at low q, the spectrum is dominated by surface scattering from grain boundaries within the powder particles. The size of the constituent grains is approximately 1 μm [16] and the power-law behaviour visible here, $I(q) \propto q^{-4}$, conforms with the predictions of scattering from smooth interfaces [19]. Because of the intense scattering power of these samples at low q, however, region i is prone to multiple scattering effects, the importance of which depends on the precise position where the beam enters the powdered sample. Owing to this uncertainty, comparisons of intensity can be unreliable in this region. In region ii, the scattering is generated by the microporous structure, and the slope to the right of the shoulder can be identified with surface scattering from the high internal surface area of the carbon [16, 18]. The features labelled iii, iv and v are in the approximate vicinity of the main diffraction peaks of graphite [20]. In the zoomed view of this highest-q region (Fig. 2b), the absence of sharp diffraction peaks is proof that the sample is entirely amorphous. The broad peaks show that the atoms are arranged in a liquid-like order.

The principle of the SAXS observations is illustrated by the example of APETA-n-hexane. Figure 3a compares

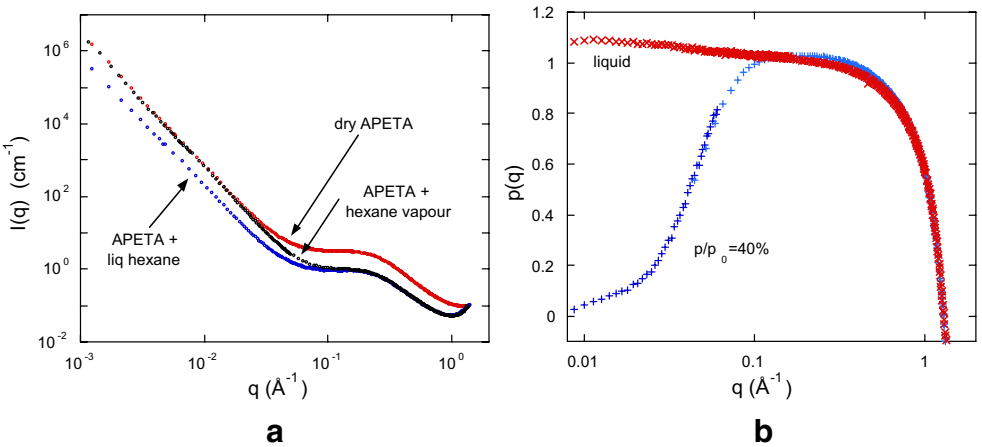

Fig. 3 **a** Scattering spectrum of APETA in air, in hexane vapour and in liquid hexane. **b** density function $p(q)$, calculated from Eq. 6, for hexane vapour and liquid hexane

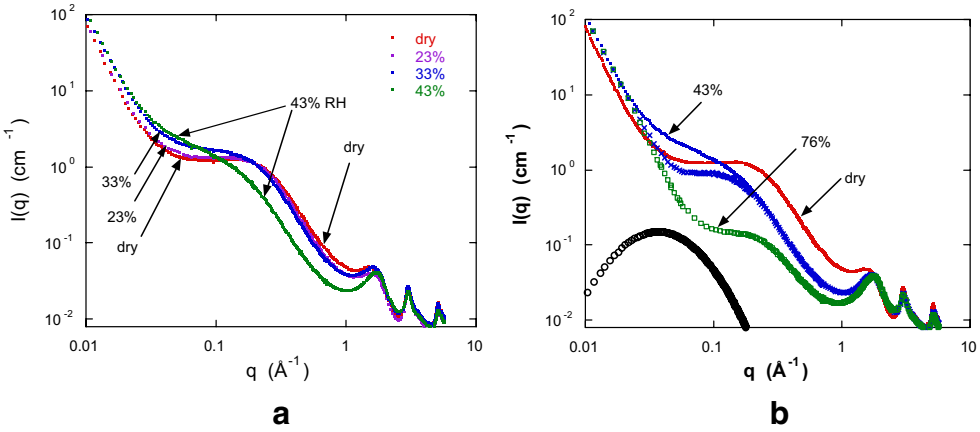

Fig. 4 **a** Scattering curves for APETA in the dry state and in water vapour at three degrees of RH; **b** SAXS from the same sample showing, in addition, spectrum at 76% RH. *Open circles* are an estimate for the third term in Eq. 3 (based on a lognormal function and divided by 10 for clarity), chosen to yield a plateau in the difference curve at $q \approx 0.1$ Å^{-1}. *Crosses* are the resulting difference curve between the full 43% curve and the lognormal function. To allow the *larger symbols* to be distinguished, only 10% of the data are displayed

three SAXS spectra from APETA: the dry sample, that exposed to hexane vapour at $p/p_0=40\%$, and that containing liquid hexane. In the higher-q regions, the intensities scattered by the vapour and liquid samples coincide and are lower than the dry sample, demonstrating that hexane is condensed in the finer pores. At low q, the opposite is true because the curves of the hexane vapour and the dry sample coincide. In the larger pores and in the grain boundaries, therefore, no condensation occurs. The values of $p(q)$ derived from Fig. 3a and Eq. 6 show that micropore filling is complete at $p/p_0=40\%$ in the high q range, i.e., in the spatial scale range 80 Å$<2\pi/q<$4.5 Å (Fig. 3b). At larger characteristic distances (smaller q), filling decreases gradually to zero. In the sample in contact with liquid hexane, on the other hand, filling is complete at all distance scales.

It has been recently shown that the pseudo-binary model gives a consistent qualitative description of pore filling in carbons of different surface chemistry both for n-hexane and for water [18]. A more systematic study was accordingly undertaken, in which SAXS measurements were performed on a set of samples in contact with water vapour over a range of values of RH.

Figure 4 shows scattering results from the lightly oxidised sample APETA in the dry state and with water vapour. Several features are notable. Firstly, in the range $0.2<q<2.1$ Å^{-1}, the curves from the humid samples lie below that of the dry curve. This means that some condensation occurs. The decrease in intensity is not uniform, however, as a much larger change in intensity occurs between 33 and 43% RH than between 0 and 33% RH. Secondly, at high q, the curves meet at $q \approx 2.1$ Å^{-1},

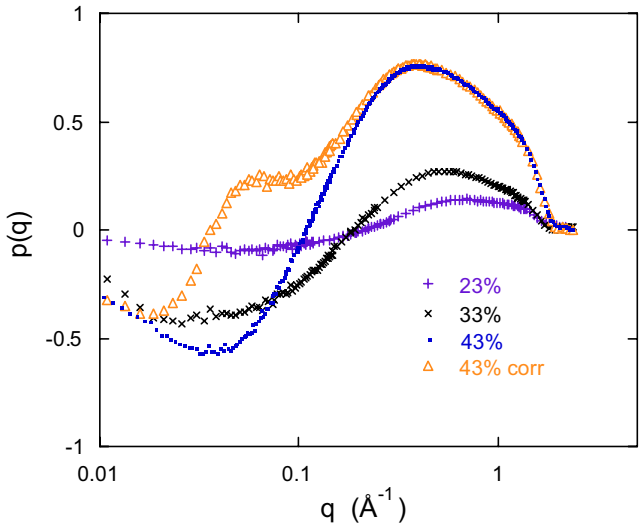

Fig. 5 Density function $p(q)$ calculated from data of Fig. 4. The negative-going region of $p(q)$ is a sign that water clusters form at all values of RH. The lognormal correction (*triangles*) proposed in Fig. 4b is seen to be inadequate at the lowest q values

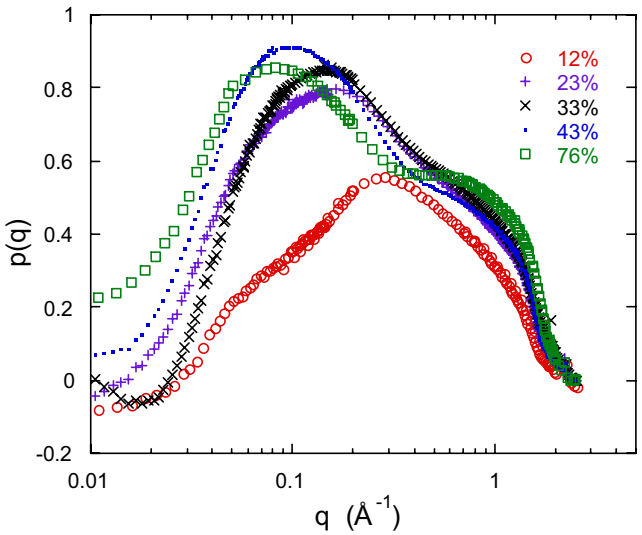

Fig. 6 Density function $p(q)$ for APETB. *Circles*, 12%; *plus signs*, 23%; *multiplication signs*, 33%; *dots*, 43%; *squares*, 76%

implying that the smallest size of the water molecule that can penetrate the carbon structure is $d_{crit}=2\pi/2.1\approx3.0$ Å, in reasonable agreement with the known critical size of the water molecule, 2.92 Å [21]. This result, however, should be treated with caution because corrections for scattering from the condensed water become significant in this region. Thirdly, at $q<0.2$ Å^{-1}, the scattering intensity from the humid samples is *greater* than in the dry system, in contradiction with Eqs. 5 and 6. The source of the extra scattering is the neglected third term in Eq. 3, which describes correlation between condensed water and its vapour. As mentioned earlier, such extra scattering will appear as a negative region in the density function $p(q)$. The variation of $p(q)$ displayed in Fig. 5 shows that, at low RH, small amounts of water condense initially in the micropores, while cluster formation develops in the more open surfaces. Between 33 and 43% RH, the amount of condensed water in the micropores starts to increase significantly, while at low q, cluster formation becomes more pronounced. The shape of the density functions in the higher q range suggests a bimodal distribution of the populated pores. A simple-minded attempt to estimate the contribution due to the clusters can be made by means of a lognormal distribution function. This yields the broad bell-shaped curve represented by open circles in Fig. 4b. This choice of function, centred at $q=0.036$ Å^{-1}, leaves the flat plateau region shown after subtraction from the experimental spectrum. As can be seen in Fig. 5, however, the approximation underestimates the broad q range of the scattering from clusters because negative values of $p(q)$ clearly persist at low q. The cluster size distribution is therefore much wider than that of a simple lognormal distribution.

The distribution of water molecules in the more oxidised sample equilibrated with various RH atmospheres is shown in Fig. 6. In the smallest pores ($q\approx1$ Å^{-1}), adsorption has already started at the lowest RH, but even at RH=76%, complete filling is not achieved. The occupation of pores of this size range is limited to less than ~60%. This is considerably less than the $p(q)$ values in the same q range for APETA. Access to the pores can be blocked by water molecules adsorbed on functional groups located at the entrance of the pores, thus hindering the passage of further adsorbates.

From 23% RH on, the relatively high occupation in the wider pores is enhanced by a cooperative mechanism, the anchorage of the water molecules being nucleated by the surface polar groups. The shape of all the curves reflects a complex distribution that is at least bimodal.

After 43%, an apparent reduction in the occupation appears above 0.6 Å^{-1}, which is probably due to the interference effect of the cross term in Eq. 3. Even in this sample, cluster formation is clearly visible in the low q range already at low RH, but it is more limited than in APETA. The positive $p(q)$ values at low q in the 76% sample indicate the disappearance of the cross term in Eq. 3 due to the coalescence of water clusters.

A detailed comparison with the water vapour adsorption isotherms and the ageing of the loaded carbon is expected to reveal further insights.

Conclusions

The presence of adsorbed molecules changes the intensity of the SAXS in a way that depends on how the pores are filled. Filling of the pores from the vapour or the liquid phase depends both on the surface treatment and on the nature of the liquid. Two carbon samples of different surface polarity were investigated. For n-hexane vapour, the dispersion interaction ensures progressive filling. The pseudo-binary model gives a consistent description of pore filling in both carbons. For water vapour, the degree of filling in the smaller pores and the cluster formation in the wider pores depend on the extent of oxidation. In the highly oxidised sample, a cooperative mechanism enhances the filling of even larger pores.

Acknowledgement The European Synchrotron Radiation Facility is gratefully acknowledged for access to the small-angle beamline BM2. We express our warm thanks to G. Bosznai and C. Rochas for their invaluable assistance. This research was supported by the EU–Hungarian Government joint fund (GVOP-3.2.2-2004-07-0006/3.0).

References

1. Lozano-Castelló D, Lillo-Ródenas MA, Cazorla-Amorós D, Linares-Solano A (2001) Carbon 39:741
2. Lillo-Ródenas MA, Lozano-Castelló D, Cazorla-Amorós D, Linares-Solano A (2001) Carbon 39:751
3. Dash RK, Yushin G, Gogotsi Y (2005) Microporous Mesoporous Mater 86:50
4. Dubinin MM (1980) Carbon 18:355
5. Mowla D, Do DD, Kaneko K (2003) In: Radovic LR (ed) Chemistry and physics of carbon, vol. 28. Marcel Dekker, New York
6. Brennan JK, Bandosz TJ, Thomson KT, Gubbins KE (2001) Colloids Surf A Physicochem Eng Asp 187–188:539
7. Lodewyckx P, Vansant EF (1999) Carbon 37:1647
8. Muller EA, Rull LF, Vega LF, Gubbins KE (1996) J Phys Chem 100:1189
9. Hoinkis E (2004) Part Part Syst Charact 21:80
10. Mitropoulos AC, Haynes JM, Richardson RM, Kanellopoulos NK (1995) Phys Rev B 52:10035
11. Ramsay JDF (1993) Pure Appl Chem 65:2169
12. Antxustegi MM, Hall PJ, Calo JM (1998) Energy Fuels 12:542
13. Lozano-Castelló D, Cazorla-Amorós D, Linares-Solano A, Hall PJ, Gascon D, Galan C (2001) Carbon 39:1343
14. Bóta A, László K, Nagy LG, Copitzky TA (1997) Langmuir 13:6502

15. László K, Czakkel O, Josepovits K, Rochas C, Geissler E (2005) Langmuir 21:8443
16. László K, Marthi K, Rochas C, Ehrburger-Dolle F, Livet F, Geissler E (2004) Langmuir 20:1321
17. László K, Tombácz E, Josepovits K (2001) Carbon 39:1217
18. László K, Geissler E (2006) Carbon 44:2437
19. Porod G (1982) In: Kratky O, Glatter O (eds) Small angle X-ray scattering. Academic Press, New York
20. Bernal JD (1924) Proc R Soc Lond A Contain Pap Math Phys Character 106:749
21. Webster CE, Drago RS, Zerner MC (1998) J Am Chem Soc 120:5509